Title:

Selective disruption of lipid peroxide homeostasis in intratumoral regulatory T cells by targeting FSP1 enhances cancer immunity

Authors:
Jesse Garcia Castillo[1], Stephanie Silveria[1], Antoine Sauquet[1], Leo Schirokauer[1], Joseph Hendricks[2,3], Hei Sook Sul[3], James A. Olzmann[2,3], and Michel DuPage[1*]

Affiliations:
[1] Division of Immunology and Molecular Medicine, Department of Molecular and Cell Biology, University of California, Berkeley, Berkeley, CA 94720, USA
[2] Division of Molecular Therapeutics, Department of Molecular and Cell Biology, University of California, Berkeley, Berkeley, CA 94720, USA
[3] Department of Nutritional Sciences and Toxicology, University of California, Berkeley, Berkeley, CA 94720, USA

*Leading Corresponding Contact: dupage@berkeley.edu

Abstract:
A burgeoning approach to treat cancer is the pharmacological induction of ferroptotic cell death of tumor cells. However, the impact of disrupting anti-ferroptotic pathways in the broader tumor microenvironment (TME), such as in immune cells, is still undefined and may complicate treatments. Here, we show that Ferroptosis Suppressor Protein 1 (FSP1/*Aifm2*) is critically required for regulatory T cell (Treg) resistance to ferroptosis and their immunosuppressive function within the TME. Compared to other canonical ferroptosis regulators such as GPX4, GCH1, and NRF2, only FSP1 was induced upon T cell activation. Deletion of *Aifm2* in all T cells, or Tregs specifically, enhanced tumor control by selectively disrupting Treg immunosuppression within tumors without inciting autoimmune pathology in mice. As opposed to deletion of *Gpx4* in all T cells, T cell deletion of *Aifm2* did not impair antigen-specific $CD8^+$ T cell responses. These results reveal a unique opportunity for targeting a regulator of ferroptosis that can not only directly target cancer cells, but also simultaneously enhance anti-cancer immune responses without inciting autoimmunity.

Main Text:

Ferroptosis, an iron-dependent form of regulated cell death driven by unchecked lipid peroxide accumulation, has emerged as a promising approach for treating therapy-resistant cancers(*1–3*). Unlike apoptosis, ferroptosis can release danger-associated

molecular patterns (DAMPs) that activate immune responses(*4*, *5*). While glutathione peroxidase 4 (GPX4) is the primary defense against ferroptosis, cancer cells often express alternative protective ferroptotic regulators, such as ferroptosis suppressor protein 1 (FSP1) and GTP cyclohydrolase 1 (GCH1), to resist GPX4 inhibition(*6*–*11*).

Regulatory T cells (Tregs), a suppressive subset of $CD4^+$ T cells, pose a major barrier to effective cancer immunotherapy by inhibiting antitumor responses through direct cell contact and the release of immunosuppressive molecules(*12*–*14*). Tregs are uniquely adapted to the nutrient-deprived and hypoxic tumor microenvironment (TME) by preferentially using oxidative phosphorylation (OXPHOS), importing lipids via CD36, and utilizing lactate and fatty acids as alternative carbon sources for their metabolism(*15*–*18*). Moreover, Tregs upregulate antioxidant pathways—including glutathione synthesis and thioredoxin—to mitigate oxidative stress and preserve their function in the TME(*19*–*21*). Although Tregs depend on GPX4 to prevent ferroptosis, inhibiting GPX4 is not a viable strategy for cancer immunotherapy as its inhibition also impairs effector $CD8^+$ and $CD4^+$ T cell survival(*22*, *23*).

In this study, we establish that FSP1/*Aifm2* is a critical effector protein for Treg resistance to ferroptosis induction *in vitro* and Treg function *in vivo* in tumors. We found that Tregs use FSP1 to prevent lipid peroxide accumulation despite having higher levels of intracellular reactive oxygen species (ROS). *Aifm2*-deficiency was sufficient to increase the sensitivity of Tregs to ferroptosis induction with GPX4 inhibition *in vitro*. *Aifm2*-deficiency in Tregs decreased the expression of proteins essential for Treg effector function, but did not impact effector T cell immune homeostasis or peripheral tolerance in young or aged mice. Total ablation of *Aifm2* in all T cells did not disrupt antitumor T cell responses but did diminish the immunosuppressive function of Tregs. These findings are significant for the translation of pharmacological FSP1 inhibitors for cancer as they show that FSP1 inhibition not only can directly sensitize cancer cells to ferroptosis, but it may also enhance immune responses to cancer by selectively blocking Treg function in the TME without generating autoimmune toxicity.

Results:

Tregs resist lipid peroxide accumulation and ferroptosis

To understand the regulation of ROS across different T cell populations, we FACS-purified naive Tregs and conventional $CD4^+$ T cells (Tconv) for activation *in vitro* and measuring their total ROS and lipid peroxide levels using fluorescent reagents detected by flow cytometry **(Fig. 1A)**. In accordance with numerous studies, we observed that Tregs had increased (~2-fold) intracellular ROS levels compared to Tconv cells(*18*, *24*) **(Fig. 1B)**. Next, we directly measured lipid peroxidation by measuring the amount of oxidized BODIPY C11 and observed that Tregs had decreased amounts of lipid peroxides compared to Tconv cells **(Fig. 1C)**. While RSL3 increased oxidized C11-

78 BODIPY in both Tregs and Tconv cells, Tconv cells increased CD11-BODIPY^{OX}
79 significantly more than Tregs **(Fig. 1D)**. Importantly, only Ferrostatin-1 (Fer-1), a radical-
80 trapping antioxidant, but not the pan-caspase inhibitor Z-VAD-FMK or RIP1 kinase
81 inhibitor Nectrostatin-1 (Nec-1) treatments reversed CD11-BODIPY^{OX} elevation, as
82 expected **(Fig. 1D)**. Improved control of lipid oxidation ultimately made Tregs more
83 resistant to ferroptotic cell death with the inhibition of GPX4 across a series of
84 concentrations of RSL3 (**Fig. 1E**). Decreased cell viability was confirmed to be due to
85 ferroptosis, as only treatment with Fer-1, but not other programmed cell death inhibitors,
86 was able to rescue cell viability **(Fig. 1F)**. Interestingly, the differences in sensitivity to
87 ferroptosis were not due to the expression of the essential Treg transcription factor
88 Foxp3, as *in vitro* induced Tregs (iTregs), were as sensitive to GPX4 inhibition as Tconv
89 cells (**Fig. 1E**)(*19*). To confirm these findings without activating or culturing T cells long
90 term *in vitro*, we isolated T cells from spleens of mice and treated them with RSL3 alone
91 or RSL3 and Fer-1 for 4 hours *ex vivo*. This revealed that while CD8^{+} and CD4^{+} Tconv
92 cells were highly sensitive to GPX4 inhibition, Tregs remained highly resistant to
93 ferroptosis *ex vivo* **(Fig. 1G)**. Therefore, despite having higher amounts of ROS, Tregs
94 reduce their accumulation of lipid peroxides, which likely increases their resistance to
95 ferroptosis.
96
97 **FSP1 expression in Tregs confers resistance to ferroptosis**
98 T cell activation increases levels of ROS, which can be tuned by the expression
99 of antioxidant genes to regulate cytosolic signaling pathways(*22*, *25–29*). Analysis of
100 gene expression by RNA-sequencing of FACS-purified Tregs and Tconv cells that were
101 naive (CD44^{lo}CD62L^{hi}) versus four days after anti-CD3/anti-CD28 *in vitro* activation,
102 demonstrated that only *Aifm2* increased expression, but not other anti-ferroptotic
103 proteins, e.g. *Gpx4*, *Gch1*, or *Nfe2l2*, upon *in vitro* T cell activation **(Fig. 2A)**(*30*). In
104 addition, a comparison of freshly sorted *in vivo* activated (CD44^{hi}CD62L^{lo}) Tregs
105 compared to naive Tregs from mice showed a similar induction of *Aifm2* in activated
106 Tregs **(Fig. 2B)**(*30*). Moreover, direct comparison of *in vitro* activated Tregs versus
107 Tconv cells revealed a 2-3 fold greater induction of *Aifm2* and *Gch1* expression, and
108 reduced expression of *Nfe2l2* and *Ascl3*, in Tregs compared to Tconvs **(Fig. 2C)**. These
109 results demonstrate that *Aifm2*/FSP1 is induced during T cell activation, but that Tregs
110 induce higher expression of *Aifm2* and *Gch1* antioxidant genes with activation, which
111 may underlie their enhanced resistance to ferroptosis.
112 While GCH1 was shown to be crucial for T cell proliferative capacity, the role of
113 FSP1 in Treg biology is unexplored(*29*). To define the role of FSP1 in Tregs, we
114 crossed mice carrying LoxP-flanked *Aifm2*^{fl} alleles with *Foxp3-GFP-hCre* to specifically
115 delete *Aifm2* in Tregs (called Treg.*Aifm2*$^{\Delta/\Delta}$ mice)(*31*). Treatment of *Aifm2*-deficient
116 Tregs with RSL3 to induce ferroptosis revealed that *Aifm2*-deficient Tregs now exhibited

117 significantly increased sensitivity to RSL3-mediated cell death compared to wildtype
118 Tregs (**Fig. 2D)**. Thus, FSP1 promotes Treg resistance to ferroptosis *in vitro*.
119 Finally, comparative gene expression analysis from human peripheral blood
120 mononuclear cells (PBMCs) confirmed that human Tregs that are activated (memory
121 Treg) also exhibit the highest expression of *Aifm2* compared both to naive Tregs as well
122 as all other activated T cell populations (**Fig. 2E-F**). These results indicate that
123 FSP1/*Aifm2* expression protects Tregs from ferroptosis and FSP1/*Aifm2* expression is
124 higher in both mouse and human activated Tregs compared to other T cell subsets.
125
126 **Treg-specific FSP1 deletion does not impact peripheral tolerance**
127 To directly test whether Treg-specific deletion of *Aifm2* disrupted Treg function *in*
128 *vivo*, we analyzed lymphoid and nonlymphoid tissues from wildtype versus
129 Treg.*Aifm2*$^{\Delta/\Delta}$ mice at early (16 weeks) and late (28 weeks) stages of life. There were no
130 changes to the frequency of CD4^{+} Tconv, CD8^{+} T, or Tregs across lymphoid organs
131 (lymph node, spleen) at any age (**Fig. 3A and Fig. S1A-B**). However, in the organ
132 tissues examined (colon, skin, lung), while CD4^{+} Tconv and CD8^{+} T cell frequencies did
133 not change in Treg.*Aifm2*$^{\Delta/\Delta}$ mice, we did note a modest reduction in Treg frequency in
134 the lung and colon of Treg.*Aifm2*$^{\Delta/\Delta}$ mice **(Fig. 3A and Fig. S1C)**. Additionally, there
135 were no changes to the activation state of CD4^{+} Tconv, CD8^{+} T, or Tregs in all tissues
136 examined (**Fig. 3B and Fig. S1D**). These data suggest that Treg-specific *Aifm2*-
137 deficiency does not increase the prevalence of autoimmunity in mice.
138 Phenotyping of the Tregs from Treg.*Aifm2*$^{\Delta/\Delta}$ mice revealed no significant
139 changes in the expression of canonical lineage defining Treg markers (i.e. CD25,
140 Foxp3, and NRP1) in either lymphoid or organ tissues **(Fig. 3C and Fig. S1E)**.
141 However, there was a significant decrease in CD73 expression on colonic and lung
142 Tregs **(Fig. 3D-E).** CD73, in conjunction with CD39, acts as an ectonucleoside that
143 breaks down ATP to generate adenosine, a critical immunosuppressive molecule
144 generated by Tregs. Interestingly, both CD73 and CD39 expression were significantly
145 decreased in the lymphoid tissues of aged mice **(Fig. S1E)**. Altogether, these results
146 show that *Aifm2*-deficiency in Tregs does not dramatically impact the frequencies or
147 phenotype of Tregs in lymphoid or non-lymphoid tissues. Thus, *Aifm2*-deficiency in
148 Tregs does not lead to a systemic breakdown in immunotolerance or organ-specific
149 autoimmunity.
150
151 **FSP1-deficiency specifically in Tregs impairs immunosuppression in response to**
152 **cancer**
153 Since the pharmacological inhibition of FSP1 in cancer cells is moving to clinical
154 trials, we next wanted to assess tumor Treg responses to the inhibition of FSP1. First,
155 we tested whether different subsets of T cells from tumors exhibited different levels of
156 resistance to ferroptosis induction, similar to experiments in Figure 1G. Here, we grew

157 MC38 colon carcinoma tumors subcutaneously for 14 days in wildtype mice, then
158 harvested tumors, made single cell suspensions, and treated all cells for four hours with
159 or without 1μM RSL3 to induce ferroptosis. Strikingly, Tregs again exhibited strong
160 resistance to the induction of ferroptosis with GPX4 inhibition as compared to Tconv
161 and $CD8^+$ T cells **(Fig. 4A)**. To test whether Treg-specific FSP1 activity promoted tumor
162 Treg resistance to ferroptosis and supported tumor growth, we compared MC38 tumor
163 growth in wildtype versus Treg.*Aifm2*$^{\Delta/\Delta}$ mice **(Fig. 4B)**(*32*). Tumor growth was
164 significantly reduced in Treg.*Aifm2*$^{\Delta/\Delta}$ mice **(Fig. 4C)**. While Treg.*Aifm2*$^{\Delta/\Delta}$ mice did not
165 exhibit changes to Treg frequencies or tumor-specific $CD8^+$ T cells in tumors (**Fig. 4D**
166 **and Fig. S2A),** Treg.*Aifm2*$^{\Delta/\Delta}$ mice did exhibit increased CD8 to Treg ratios in tumors,
167 indicative of a selective impact on Tregs compared to effector T cells in tumors with
168 FSP1-deficiency in Tregs (**Fig. 4D)**. In addition, we did not observe altered expression
169 of the exhaustion markers PD-1 or LAG-3 in $CD8^+$ T cells in Treg.*Aifm2*$^{\Delta/\Delta}$ mice (**Fig.**
170 **S2B**). Importantly, to demonstrate that the reduction in tumor growth was due to the
171 accumulation of lipid peroxides in FSP1-deficient Tregs, we treated wildtype and
172 Treg.*Aifm2*$^{\Delta/\Delta}$ tumor-bearing mice with the radical trapping antioxidant liproxstatin-1
173 (Lip-1), a ferroptosis inhibitor that is functional *in vivo in mice(33)* (**Fig. 4E**). Lip-1
174 treatment restored tumor growth in Treg.*Aifm2*$^{\Delta/\Delta}$ mice, while Lip-1 treatment had no
175 effect on tumor growth in wildtype mice (**Fig. 4F**). These results indicate that FSP1
176 activity in Tregs is required to control their accumulation of lipid peroxides within the
177 TME, and disruption of FSP1 activity can release immunosuppression by Tregs and
178 promote better tumor control.
179
180 **FSP1-deficiency in all T cells enhances T cell responses to infection and cancer**
181 T cell deficiency for *Gpx4*- or *Gch-1* was recently shown to negatively impact T
182 cell responses in several disease settings(*23*, *29*, *34*). To test if *Aifm2*-deficiency also
183 impacts all T cell responses, which would occur with pharmacological inhibition for
184 cancer treatment, we generated *Aifm2*-deficient T cell mice (*CD4-Cre;Aifm2*$^{fl/fl}$, called
185 *T.Aifm2*$^{\Delta/\Delta}$) and infected these mice with *Listeria monocytogenes*, an intracellular
186 pathogen known for stimulating a robust $CD8^+$ T cell response (**Fig. S3A**)(*35*, *36*).
187 Importantly, *T.Aifm2*$^{\Delta/\Delta}$ mice had no deficiency in bacterial control, as there was no
188 difference in bacterial CFUs recovered from spleens or livers of wildtype versus
189 *T.Aifm2*$^{\Delta/\Delta}$ six days post infection (**Fig. S3B**). Upon *Listeria* infection, we observed a
190 decrease in the frequency of Tregs as a percentage of $CD4^+$ T conv cells, as well as of
191 total $CD45^+$ immune cells, in *T.Aifm2*$^{\Delta/\Delta}$ (**Fig. S3C**). The frequency of total $CD8^+$ T cells,
192 *Listeria*-specific $CD8^+$ T cells, or $CD4^+$ Tconv cell populations, however, did not change
193 (**Fig. S3D-F**).
194 Next, to test the impact of deleting *Aifm2* in all T cells, as would happen with a
195 pharmacological FSP1 inhibitor, in the setting of cancer, we implanted MC38 tumors
196 into wildtype versus *T.Aifm2*$^{\Delta/\Delta}$ mice and measured tumor growth (**Fig. 5A**). Tumor

growth was significantly decreased in mice harboring *Aifm2*-deficient T cells (**Fig. 5B**). While there was no change in the frequency of Tregs in MC38 tumors, there was an increase in the CD8:Treg ratios in tumors from *T.Aifm2*$^{\Delta/\Delta}$ compared to wildtype mice, as observed with Treg-specific *Aifm2*-deficiency (**Fig. 5C-D**)(*37*, *38*). Assessment of CD8^{+} T cell exhaustion in tumors by staining for both PD-1 and Lag-3 proteins showed no changes in total CD8^{+} T cells **(Fig. 5E)**. However, tumor-specific CD8^{+} T cells, while unchanged in total frequencies, exhibited decreased frequencies of PD-1^{+}Lag3^{+} MuLV/H2K^{b+} CD8^{+} T cells (**Fig. 5F**)(*39*). These results starkly contrast with the consequences of T cell deficiencies in other antioxidant genes, i.e. *Gpx4* or *Gch1*, where deficient T cells completely lost their capacities to control infections or cancer(*23*, *29*). Instead, deficiency for FSP1/*Aifm2* in all T cells completely preserves CD8^{+} and CD4^{+} Tconv cell function while potently disrupting the function of Tregs.

Discussion:

In this study, we demonstrate that FSP1 (*Aifm2*) plays a critical role, and unique role amongst T cells, in sustaining Treg function within tumors. Unlike other ferroptosis resistance factors such as GPX4, which are essential for proper T cell function during infections or cancer, FSP1 appears to be selectively required for Tregs without compromising effector T cell responses. We show that FSP1 expression is induced during T cell activation, distinguishing it from other ferroptosis regulators like GPX4, GCH1, or NRF2. Our data indicate that FSP1 supports Treg survival and suppressive function by limiting lipid peroxide accumulation despite high levels of ROS generation in Tregs. This suggests that increased FSP1 expression in Tregs may have evolved to prevent sublethal oxidative damage that would otherwise kill or impair Tregs.

These findings reveal a novel paradigm in which targeting FSP1 may specifically modulate Treg-mediated immunosuppression in cancer without affecting effector T cells. In contrast to GPX4-targeted approaches, which can dampen overall T cell responses and carry a narrow therapeutic window due to GPX4's essential role in multiple tissues, inhibition of FSP1 appears to selectively compromise Treg function(*23*, *34*, *40*, *41*). In addition, Tregs are sensitive to specific antioxidant pathway activity as the genetic deletion of KEAP1 leads to loss of Treg lineage identity that leads to spontaneous autoimmunity due to hyperactivation of NRF2 and uncontrolled induction of antioxidant pathways(*42*). Our tumor models showed that genetic ablation of FSP1 in T cells resulted in better tumor control, potentially due to a reduction in Treg suppressive capacity and a concomitant decrease in canonical exhaustion markers (e.g., PD-1, Lag3) on tumor-specific CD8^{+} T cells(*43*).

The implications of these findings are significant. By specifically targeting FSP1, it may be possible to alleviate the immunosuppressive effects of Tregs within the TME, thereby enhancing the efficacy of cancer immunotherapies. Moreover, FSP1 inhibition exhibits great potential to synergize with immune checkpoint blockade (e.g., anti-PD-1

therapies) and cellular immunotherapies such as CAR T cells by preventing T cell exhaustion and preserving cytotoxic function. PD-1 blockade has also been shown to induce IFN-γ production by $CD8^+$ T cells, which induced ferroptosis in cancer cells directly by impacting the lipid composition through Ascl4 expression(*44*). Thus, this dual approach, targeting tumor cells directly through ferroptosis induction while simultaneously modulating Treg function, could offer a much broader therapeutic strategy for treating cancer.

Our study also underscores the importance of metabolic regulation in Treg biology. Tregs exhibit a unique metabolic profile characterized by a reliance on oxidative phosphorylation and fatty acid utilization, which supports their survival in the nutrient-deprived, hypoxic TME(*15*–*17*). Despite high ROS levels due to these forms of metabolism, Tregs maintain low lipid peroxide accumulation, in part by maintaining higher expression of FSP1. Disrupting this balance through FSP1 inhibition leads to functional defects in Tregs without appearing to cause their complete elimination in vivo, which is preferable for preserving immune homeostasis.

In conclusion, our results position FSP1 as a Treg-specific ferroptosis regulator and a promising therapeutic target for enhancing cancer immunity. By selectively modulating FSP1 activity, it may be possible to reduce Treg-mediated suppression in tumors, preserve effector T cell responses, and ultimately improve the outcomes of cancer immunotherapy. Future studies should focus on translating these findings into pharmacological interventions, as well as exploring the potential of FSP1-targeting strategies in combination with existing immunotherapies to achieve synergistic effects.

Materials and Methods:

Mice

CD4-Cre mice were obtained from Jackson laboratories (JAX:022071) and bred in house. Foxp3-GFP-hCre mice were obtained from Jackson laboratories (JAX:023161) and bred in house. *Aifm2*^{fl} mice were generated as described(*31*). For tumor studies, syngeneic C57BL/6J mice were inoculated with 5.0×10^5 MC38 in PBS subcutaneously. Tumor measurements were performed blindly across the entire experiment by a single operator measuring three dimensions of the tumor with calipers three times per week. For in vivo liproxstatin treatments (Selleck Chemicals), mice were injected intraperitoneally with 10mg/kg of liproxstatin-1 dissolved in DMSO and diluted in PEG300, Tween-80, and dH2O. All the experiments were conducted according to the Institutional Animal Care and Use Committee guidelines of the University of California, Berkeley.

Cell lines

MC38 cell lines were kindly provided by Dr. Jeff Bluestone's lab(*45*). All cell lines were maintained in DMEM (GIBCO) supplemented with 10% FBS, sodium pyruvate (GIBCO),

277 10mM HEPES (GIBCO), and penicillin-streptomycin (GIBCO). Tumor cells were grown
278 at 37℃ with 5% CO_2.
279
280 **Listeria monocytogenes strains**
281 All strains of L. monocytogenes were derived from the wild-type 10403S strain. All
282 strains were cultured in filter-sterilized nutrient-rich Brain Heart Infusion (BHI) media
283 (BD Biosciences) containing 200 µg/mL streptomycin (Sigma-Aldrich).
284
285 **Intravenous and Intratumoral Listeria infection**
286 Overnight cultures were grown in BHI + 200 µg/mL streptomycin at 30℃. The following
287 day, bacteria were grown to logarithmic phase by diluting the overnight culture in fresh
288 BHI + 200 µg/mL streptomycin and culturing at 37℃ shaking. Log-phase bacteria were
289 washed and frozen in 9% glycerol/PBS. For intravenous infections, frozen stocks were
290 diluted in PBS to infect via the tail vein with $5x10^3$ CFU log-phase bacteria. The mice
291 were euthanized 6 days after intravenous injections and organs were collected for CFU
292 or flow analysis.
293
294 **Primary Treg and T cell culture**
295 Spleens and lymph nodes were collected from Foxp3-GFP-hCre;$R26^{LSL\text{-}RFP}$; *Aifm2*$^{+/+}$,
296 Foxp3-GFP-hCre;$R26^{LSL\text{-}RFP}$; *Aifm2*$^{\Delta/\Delta}$, CD4-Cre;*Aifm2*$^{+/+}$ or CD4-Cre;*Aifm2*$^{\Delta/\Delta}$. Single
297 cell suspensions were generated and enriched for CD4+ T cells by negative selection
298 using EasySep magnetic bead kit (STEMCELL Technologies) and stained with anti-
299 mouse CD4 (RM4-5, BioLegend), anti-CD62L (MEL1-14, Biolegend), anti-CD8 (53-6.7,
300 Biolegend), anti-CD25 (PC61, BioLegend), anti-CD357 (GITR) (DTA-1, Biolegend).
301 Naïve Treg cells ($CD4^+Foxp3GFP^+RFP^+CD62L^+$ or $CD4^+CD25^+GITR^+CD62L^+$) and
302 naive $CD4^+$ T cells ($CD4^+CD62L^+Foxp3GFP^-RFP^-$ or $CD4^+CD62L^+GITR^-CD25^-$) were
303 sorted using an Aria Fusion sorter (BD Biosciences) with a 70µm nozzle. Cells were
304 activated with anti-CD3 and anti-CD28 coated beads (Dynabeads Mouse T-Activator
305 CD3/CD28, Invitrogen) at a ratio of 1:1 for Tconv or 1:3 ratio for Tregs (cell:bead). Cells
306 were kept at a concentration of 10^6 cells/ml in DMEM medium supplemented with 10%
307 FBS, non-essential amino acids, sodium pyruvate, L-glutamine, HEPES, and β-ME, and
308 cells cultured more than 24 hr were supplemented with 200–2,000 IU/ml recombinant
309 human IL-2 (NIH).
310
311 **Tissue Collection and preparation for Flow cytometry**
312 Flow cytometry was performed on an BD LSR Fortessa X20 (BD Biosciences), CyTEK
313 Aurora (CyTEK Biosciences) or LSRFortessa (BD Biosciences) and datasets were
314 analyzed using FlowJo software (Tree Star). Single cell suspensions were prepared in
315 ice-cold FACS buffer (PBS with 2mM EDTA and 1% BS) and subjected to red blood cell
316 lysis using ACK buffer (150mM NH_4Cl, 10mM $KHCO_3$, 0.1mM Na2EDTA, pH7.3). Dead

cells were stained with Live/Dead Fixable Blue or Aqua Dead Cell Stain kit (Molecular Probes) in PBS at 4℃. Cell surface antigens were stained at 4℃ using a mixture of fluorophore-conjugated antibodies. Surface marker stains for murine samples were carried out with anti-mouse CD3 (17A2, BioLegend), anti-mouse CD4 (RM4-5, BioLegend), anti-mouse CD8a (53-6.7, BioLegend), anti-mouse, CD44 (IM7, BioLeged), anti-mouse CD45 (30-F11, BioLegend), anti-H-2K^b MuLV p15E Tetramer-KSPWFTTL (MBL), anti-H-2K^b SIINFEKL Tetramer (NIH Tetramer Core) in PBS, 0.5% BSA. Cells were fixed using the eBioscience Foxp3/Transcription Factor staining buffer set (eBioscience), prior to intracellular staining. Intracellular staining was performed using anti-mouse Foxp3 (FJK-16S, eBioscience) at 4℃, according to manufacturer's instructions. Cells were resuspended in PBS and filtered through a 70-μm nylon mesh before data acquisition. Datasets were analyzed using FlowJo software (Tree Star).

Statistical Methods

p values were obtained from unpaired two-tailed Student's t tests for all statistical comparisons between two groups, and data were displayed as mean ± SEMs or mean ± SD. For multiple comparisons, one-way ANOVA or two-way ANOVA was used. For tumor growth curves, two-way ANOVA was used with Sidak's multiple comparisons test performed at each time point or by multiple regression analysis p values are denoted in figures by *$p < 0.05$, **$p < 0.01$, ***$p < 0.001$, and ****$p < 0.0001$.

References:

1. S. J. Dixon, J. A. Olzmann, The cell biology of ferroptosis. *Nat Rev Mol Cell Biol* **25**, 424–442 (2024).

2. T. Nakamura, M. Conrad, Exploiting ferroptosis vulnerabilities in cancer. *Nature Cell Biology* **26**, 1407–1419 (2024).

3. K. Hadian, B. R. Stockwell, The therapeutic potential of targeting regulated non-apoptotic cell death. *Nature Reviews Drug Discovery* **22**, 723–742 (2023).

4. The release and activity of HMGB1 in ferroptosis. *Biochemical and Biophysical Research Communications* **510**, 278–283 (2019).

5. G. Kroemer, C. Galassi, L. Zitvogel, L. Galluzzi, Immunogenic cell stress and death. *Nature Immunology* **23**, 487–500 (2022).

6. K. Bersuker, J. M. Hendricks, Z. Li, L. Magtanong, B. Ford, P. H. Tang, M. A. Roberts, B. Tong, T. J. Maimone, R. Zoncu, M. C. Bassik, D. K. Nomura, S. J. Dixon, J. A. Olzmann, The CoQ oxidoreductase FSP1 acts parallel to GPX4 to inhibit ferroptosis. *Nature* **575**, 688–692 (2019).

7. S. Doll, F. P. Freitas, R. Shah, M. Aldrovandi, M. C. da Silva, I. Ingold, A. Goya Grocin, T. N. Xavier da Silva, E. Panzilius, C. H. Scheel, A. Mourão, K. Buday, M.

355 Sato, J. Wanninger, T. Vignane, V. Mohana, M. Rehberg, A. Flatley, A. Schepers,
356 A. Kurz, D. White, M. Sauer, M. Sattler, E. W. Tate, W. Schmitz, A. Schulze, V.
357 O'Donnell, B. Proneth, G. M. Popowicz, D. A. Pratt, J. P. F. Angeli, M. Conrad,
358 FSP1 is a glutathione-independent ferroptosis suppressor. *Nature* **575**, 693–698
359 (2019).

360 8. V. A. N. Kraft, C. T. Bezjian, S. Pfeiffer, L. Ringelstetter, C. Müller, F. Zandkarimi, J.
361 Merl-Pham, X. Bao, N. Anastasov, J. Kössl, S. Brandner, J. D. Daniels, P. Schmitt-
362 Kopplin, S. M. Hauck, B. R. Stockwell, K. Hadian, J. A. Schick, GTP
363 Cyclohydrolase 1/Tetrahydrobiopterin Counteract Ferroptosis through Lipid
364 Remodeling. *ACS Central Science*, doi: 10.1021/acscentsci.9b01063 (2019).

365 9. E. Mishima, J. Ito, Z. Wu, T. Nakamura, A. Wahida, S. Doll, W. Tonnus, P.
366 Nepachalovich, E. Eggenhofer, M. Aldrovandi, B. Henkelmann, K.-I. Yamada, J.
367 Wanninger, O. Zilka, E. Sato, R. Feederle, D. Hass, A. Maida, A. S. D. Mourão, A.
368 Linkermann, E. K. Geissler, K. Nakagawa, T. Abe, M. Fedorova, B. Proneth, D. A.
369 Pratt, M. Conrad, A non-canonical vitamin K cycle is a potent ferroptosis
370 suppressor. *Nature* **608**, 778–783 (2022).

371 10. D.-Y. Jin, X. Chen, Y. Liu, C. M. Williams, L. C. Pedersen, D. W. Stafford, J.-K. Tie,
372 A genome-wide CRISPR-Cas9 knockout screen identifies FSP1 as the warfarin-
373 resistant vitamin K reductase. *Nat Commun* **14**, 828 (2023).

374 11. M. Soula, R. A. Weber, O. Zilka, H. Alwaseem, K. La, F. Yen, H. Molina, J. Garcia-
375 Bermudez, D. A. Pratt, K. Birsoy, Metabolic determinants of cancer cell sensitivity
376 to canonical ferroptosis inducers. *Nat Chem Biol* **16**, 1351–1360 (2020).

377 12. Primary, Adaptive, and Acquired Resistance to Cancer Immunotherapy. *Cell* **168**,
378 707–723 (2017).

379 13. J. B. Wing, A. Tanaka, S. Sakaguchi, Human FOXP3 Regulatory T Cell
380 Heterogeneity and Function in Autoimmunity and Cancer. *Immunity* **50**, 302–316
381 (2019).

382 14. M. A. Moreno Ayala, Z. Li, M. DuPage, Treg programming and therapeutic
383 reprogramming in cancer. *Immunology* **157**, 198–209 (2019).

384 15. A. Angelin, L. Gil-de-Gómez, S. Dahiya, J. Jiao, L. Guo, M. H. Levine, Z. Wang, W.
385 J. Quinn 3rd, P. K. Kopinski, L. Wang, T. Akimova, Y. Liu, T. R. Bhatti, R. Han, B.
386 L. Laskin, J. A. Baur, I. A. Blair, D. C. Wallace, W. W. Hancock, U. H. Beier, Foxp3
387 Reprograms T Cell Metabolism to Function in Low-Glucose, High-Lactate
388 Environments. *Cell Metab* **25**, 1282–1293.e7 (2017).

389 16. R. Newton, B. Priyadharshini, L. A. Turka, Immunometabolism of regulatory T cells.
390 *Nature Immunology* **17**, 618–625 (2016).

391 17. J. Miska, C. Lee-Chang, A. Rashidi, M. E. Muroski, A. L. Chang, A. Lopez-Rosas,
392 P. Zhang, W. K. Panek, A. Cordero, Y. Han, A. U. Ahmed, N. S. Chandel, M. S.

393 Lesniak, HIF-1α Is a Metabolic Switch between Glycolytic-Driven Migration and
394 Oxidative Phosphorylation-Driven Immunosuppression of Tregs in Glioblastoma.
395 *Cell Rep* **27**, 226–237.e4 (2019).

396 18. T. Maj, W. Wang, J. Crespo, H. Zhang, W. Wang, S. Wei, L. Zhao, L. Vatan, I.
397 Shao, W. Szeliga, C. Lyssiotis, J. R. Liu, I. Kryczek, W. Zou, Oxidative stress
398 controls regulatory T cell apoptosis and suppressor activity and PD-L1-blockade
399 resistance in tumor. *Nature Immunology* **18**, 1332–1341 (2017).

400 19. H. Kurniawan, D. G. Franchina, L. Guerra, L. Bonetti, L. Soriano-Baguet, M.
401 Grusdat, L. Schlicker, O. Hunewald, C. Dostert, M. P. Merz, C. Binsfeld, G. S.
402 Duncan, S. Farinelle, Y. Nonnenmacher, J. Haight, D. D. Gupta, A. Ewen, R.
403 Taskesen, R. Halder, Y. Chen, C. Jäger, M. Ollert, P. Wilmes, V. Vasiliou, I. S.
404 Harris, C. B. Knobbe-Thomsen, J. D. Turner, T. W. Mak, M. Lohoff, J. Meiser, K.
405 Hiller, D. Brenner, Glutathione restricts serine metabolism to preserve regulatory T
406 cell function. *Cell metabolism* **31**, 920 (2020).

407 20. Z. Yan, S. K. Garg, R. Banerjee, Regulatory T cells interfere with glutathione
408 metabolism in dendritic cells and T cells. *J Biol Chem* **285**, 41525–41532 (2010).

409 21. Z. Yan, S. K. Garg, J. Kipnis, R. Banerjee, Extracellular redox modulation by
410 regulatory T cells. *Nat Chem Biol* **5**, 721–723 (2009).

411 22. C. Xu, S. Sun, T. Johnson, R. Qi, S. Zhang, J. Zhang, K. Yang, The glutathione
412 peroxidase Gpx4 prevents lipid peroxidation and ferroptosis to sustain Treg cell
413 activation and suppression of antitumor immunity. *Cell Reports* **35** (2021).

414 23. M. Matsushita, S. Freigang, C. Schneider, M. Conrad, G. W. Bornkamm, M. Kopf, T
415 cell lipid peroxidation induces ferroptosis and prevents immunity to infection. *J Exp*
416 *Med* **212**, 555–568 (2015).

417 24. S. E. Weinberg, B. D. Singer, E. M. Steinert, C. A. Martinez, M. M. Mehta, I.
418 Martínez-Reyes, P. Gao, K. A. Helmin, H. Abdala-Valencia, L. A. Sena, P. T.
419 Schumacker, L. A. Turka, N. S. Chandel, Mitochondrial complex III is essential for
420 suppressive function of regulatory T cells. *Nature* **565**, 495–499 (2019).

421 25. M. P. Murphy, R. M. Siegel, Mitochondrial ROS fire up T cell activation. *Immunity*
422 **38**, 201–202 (2013).

423 26. S. H. Jackson, S. Devadas, J. Kwon, L. A. Pinto, M. S. Williams, T cells express a
424 phagocyte-type NADPH oxidase that is activated after T cell receptor stimulation.
425 *Nat Immunol* **5**, 818–827 (2004).

426 27. J. Kwon, K. E. Shatynski, H. Chen, S. Morand, X. de Deken, F. Miot, T. L. Leto, M.
427 S. Williams, The nonphagocytic NADPH oxidase Duox1 mediates a positive
428 feedback loop during T cell receptor signaling. *Sci Signal* **3**, ra59 (2010).

429 28. L. A. Sena, S. Li, A. Jairaman, M. Prakriya, T. Ezponda, D. A. Hildeman, C.-R.

430 Wang, P. T. Schumacker, J. D. Licht, H. Perlman, P. J. Bryce, N. S. Chandel,
431 Mitochondria are required for antigen-specific T cell activation through reactive
432 oxygen species signaling. *Immunity* **38**, 225–236 (2013).

433 29. S. J. F. Cronin, C. Seehus, A. Weidinger, S. Talbot, S. Reissig, M. Seifert, Y.
434 Pierson, E. McNeill, M. S. Longhi, B. L. Turnes, T. Kreslavsky, M. Kogler, D.
435 Hoffmann, M. Ticevic, D. da Luz Scheffer, L. Tortola, D. Cikes, A. Jais, M.
436 Rangachari, S. Rao, M. Paolino, M. Novatchkova, M. Aichinger, L. Barrett, A.
437 Latremoliere, G. Wirnsberger, G. Lametschwandtner, M. Busslinger, S. Zicha, A.
438 Latini, S. C. Robson, A. Waisman, N. Andrews, M. Costigan, K. M. Channon, G.
439 Weiss, A. V. Kozlov, M. Tebbe, K. Johnsson, C. J. Woolf, J. M. Penninger, The
440 metabolite BH4 controls T cell proliferation in autoimmunity and cancer. *Nature*
441 **563**, 564–568 (2018).

442 30. D. Wang, J. Quiros, K. Mahuron, C.-C. Pai, V. Ranzani, A. Young, S. Silveria, T.
443 Harwin, A. Abnousian, M. Pagani, M. D. Rosenblum, F. Van Gool, L. Fong, J. A.
444 Bluestone, M. DuPage, Targeting EZH2 Reprograms Intratumoral Regulatory T
445 Cells to Enhance Cancer Immunity. *Cell Rep* **23**, 3262–3274 (2018).

446 31. H. P. Nguyen, D. Yi, F. Lin, J. A. Viscarra, C. Tabuchi, K. Ngo, G. Shin, A. Y.-F.
447 Lee, Y. Wang, H. S. Sul, Aifm2, a NADH Oxidase, Supports Robust Glycolysis and
448 Is Required for Cold- and Diet-Induced Thermogenesis. *Mol Cell* **77**, 600–617.e4
449 (2020).

450 32. M. A. Moreno Ayala, T. F. Campbell, C. Zhang, N. Dahan, A. Bockman, V.
451 Prakash, L. Feng, T. Sher, M. DuPage, CXCR3 expression in regulatory T cells
452 drives interactions with type I dendritic cells in tumors to restrict CD8+ T cell
453 antitumor immunity. *Immunity* **56**, 1613–1630.e5 (2023).

454 33. J. Li, J. Liu, Z. Zhou, R. Wu, X. Chen, C. Yu, B. Stockwell, G. Kroemer, R. Kang, D.
455 Tang, Tumor-specific GPX4 degradation enhances ferroptosis-initiated antitumor
456 immune response in mouse models of pancreatic cancer. *Science Translational*
457 *Medicine*, doi: 10.1126/scitranslmed.adg3049 (2023).

458 34. Y. Yao, Z. Chen, H. Zhang, C. Chen, M. Zeng, J. Yunis, Y. Wei, Y. Wan, N. Wang,
459 M. Zhou, C. Qiu, Q. Zeng, H. S. Ong, H. Wang, F. V. Makota, Y. Yang, Z. Yang, N.
460 Wang, J. Deng, C. Shen, Y. Xia, L. Yuan, Z. Lian, Y. Deng, C. Guo, A. Huang, P.
461 Zhou, H. Shi, W. Zhang, H. Yi, D. Li, M. Xia, J. Fu, N. Wu, J. B. de Haan, N. Shen,
462 W. Zhang, Z. Liu, D. Yu, Selenium–GPX4 axis protects follicular helper T cells from
463 ferroptosis. *Nature Immunology* **22**, 1127–1139 (2021).

464 35. A. Chávez-Arroyo, D. A. Portnoy, Why is Listeria monocytogenes such a potent
465 inducer of CD8+ T-cells? *Cell Microbiol* **22**, e13175 (2020).

466 36. A. Benson, S. Murray, P. Divakar, N. Burnaevskiy, R. Pifer, J. Forman, F.
467 Yarovinsky, Microbial infection-induced expansion of effector T cells overcomes the
468 suppressive effects of regulatory T cells via an IL-2 deprivation mechanism. *J*
469 *Immunol* **188**, 800–810 (2012).

470 37. J. D. French, Z. J. Weber, D. L. Fretwell, S. Said, J. P. Klopper, B. R. Haugen,
471 Tumor-associated lymphocytes and increased FoxP3+ regulatory T cell frequency
472 correlate with more aggressive papillary thyroid cancer. *J Clin Endocrinol Metab* **95**,
473 2325–2333 (2010).

474 38. H. Ohtani, O. Yoshie, Morphometric analysis of the balance between CXCR3+ T
475 cells and FOXP3+ regulatory T cells in lymphocyte-rich and conventional gastric
476 cancers. *Virchows Arch* **456**, 615–623 (2010).

477 39. B. J. Hos, M. G. M. Camps, J. van den Bulk, E. Tondini, T. C. van den Ende, D.
478 Ruano, K. Franken, G. M. C. Janssen, A. Ru, D. V. Filippov, R. Arens, P. A. van
479 Veelen, N. Miranda, F. Ossendorp, Identification of a neo-epitope dominating
480 endogenous CD8 T cell responses to MC-38 colorectal cancer. *Oncoimmunology*
481 **9**, 1673125 (2019).

482 40. L. Chen, W. S. Hambright, R. Na, Q. Ran, Ablation of the Ferroptosis Inhibitor
483 Glutathione Peroxidase 4 in Neurons Results in Rapid Motor Neuron Degeneration
484 and Paralysis. *J Biol Chem* **290**, 28097–28106 (2015).

485 41. J. P. Friedmann Angeli, M. Schneider, B. Proneth, Y. Y. Tyurina, V. A. Tyurin, V. J.
486 Hammond, N. Herbach, M. Aichler, A. Walch, E. Eggenhofer, D. Basavarajappa, O.
487 Rådmark, S. Kobayashi, T. Seibt, H. Beck, F. Neff, I. Esposito, R. Wanke, H.
488 Förster, O. Yefremova, M. Heinrichmeyer, G. W. Bornkamm, E. K. Geissler, S. B.
489 Thomas, B. R. Stockwell, V. B. O'Donnell, V. E. Kagan, J. A. Schick, M. Conrad,
490 Inactivation of the ferroptosis regulator Gpx4 triggers acute renal failure in mice.
491 *Nat Cell Biol* **16**, 1180–1191 (2014).

492 42. P. Klemm, A. Rajendiran, A. Fragoulis, C. Wruck, A. Schippers, N. Wagner, T.
493 Bopp, K. Tenbrock, K. Ohl, Nrf2 expression driven by Foxp3 specific deletion of
494 Keap1 results in loss of immune tolerance in mice. *Eur J Immunol* **50**, 515–524
495 (2020).

496 43. S.-R. Woo, M. E. Turnis, M. V. Goldberg, J. Bankoti, M. Selby, C. J. Nirschl, M. L.
497 Bettini, D. M. Gravano, P. Vogel, C. L. Liu, S. Tangsombatvisit, J. F. Grosso, G.
498 Netto, M. P. Smeltzer, A. Chaux, P. J. Utz, C. J. Workman, D. M. Pardoll, A. J.
499 Korman, C. G. Drake, D. A. A. Vignali, Immune inhibitory molecules LAG-3 and PD-
500 1 synergistically regulate T-cell function to promote tumoral immune escape.
501 *Cancer Res* **72**, 917–927 (2012).

502 44. CD8+ T cells and fatty acids orchestrate tumor ferroptosis and immunity via
503 ACSL4. *Cancer Cell* **40**, 365–378.e6 (2022).

504 45. J. T. Sockolosky, E. Trotta, G. Parisi, L. Picton, L. L. Su, A. C. Le, A. Chhabra, S. L.
505 Silveria, B. M. George, I. C. King, M. R. Tiffany, K. Jude, L. V. Sibener, D. Baker, J.
506 A. Shizuru, A. Ribas, J. A. Bluestone, K. C. Garcia, Selective targeting of
507 engineered T cells using orthogonal IL-2 cytokine-receptor complexes. *Science*
508 **359**, 1037–1042 (2018).

Acknowledgments:
We thank Hector Nolla, Alma Valleros, Kartoosh Heydari and Anita Wong Lin of the UC Berkeley Cancer Research Laboratory Flow Cytometry Facility. This research was supported by 1DP2CA247830-01 from the National Institutes of Health (NCI), R01GM112948 from the National Institutes of Health, and C23CR5612 from the UC CRCC Cancer Research Coordinating Committee. M.D. is a Pew-Stewart Scholar and a St. Baldrick's Scholar with generous support from Hope with Hazel. J.G.C is a HHMI Gilliam Fellow. J.A.O is a Chan-Zuckerberg investigator.

Author Contributions:
Conceptualization and Methodology, M.D., J.A.O., J.G.C.; Investigation, J.G.C., S.S., A.S., L.S., J.H., J.A.O., and M.D.; Writing – Original Draft, J.G.C., M.D., J.A.O.; Writing – Review & Editing, J.G.C., M.D., J.A.O., S.S.; Supervision, M.D., J.A.O., J.G.C.; Funding Acquisition, M.D., J.A.O.

Resource Availability

Lead Contact
Further information and requests for resources and reagents should be directed to and will be fulfilled by the lead contact, Michel DuPage (dupage@berkeley.edu).

Materials availability
Listeria monocytogenes strains used in the study will be made available from the lead contact upon request.

Declaration of Interests:
J.A.O. is a member of the scientific advisory board for Vicinitas Therapeutics and has patent applications related to ferroptosis.

Supplementary Materials
Materials and Methods
Figures S1 to S3

Figure Legends:
Fig. 1 | Regulatory T cells (Tregs) naturally resist lipid peroxide accumulation and ferroptosis. (A) Schematic for *in vitro* T cell assays. (B) Representative flow plots (left) and quantification (right) of bulk reactive oxygen species (ROS) by CellROX™ staining in Tregs versus conventional $CD4^+$ T cells (Tconv) after activation and culture for 4 days *in vitro*. Data pooled from 5 independent experiments. (C) Representative flow plots for detection of oxidized C11-BODIPY in Tregs versus Tconv that were activated for 4 days *in vitro*. (D) Quantification of oxidized C11-BODIPY in Tregs versus Tconv cells *in vitro*

549 +/- 1μM RSL3 in combination with 2μM Fer-1, 100μM Z-VAD-FMK, or 10μM Nec-1.
550 Data pooled from 3 experiments. (E) Cell viability of Tregs (nTregs), $CD4^+$ Tconv, and
551 induced Tregs ($Foxp3^+$ iTregs) treated with the indicated concentrations of RSL3 for 4
552 hours. Representative data from 2 independent experiments. (F) Cell viability of Tregs
553 versus $CD4^+$ Tconv treated *in vitro* +/- 1μM RSL3 in combination with 2μM Fer-1,
554 100μM Z-VAD-FMK, or 10μM Nec-1. Data pooled from 2 experiments. (G) Frequencies
555 of viable $CD8^+$ T (left), $CD4^+$ Tconv (middle), and Tregs (right) from spleen plotted as
556 the percent of $CD45^+$ cells +/- 1μM RSL3 and 2μM Fer-1. Data from n=7 mice. For all
557 plots, **P<0.05, **P<0.01, ***P<0.001 by two-way ANOVA (D-F) or one-way ANOVA
558 (G), or student t-test (B), mean ± s.d (B, D-F) or mean ± s.e.m (G).
559
560 **Fig. 2 | FSP1 drives Treg resistance to ferroptosis.** (A) Fold-change expression of
561 indicated anti-ferroptotic genes in naive ($CD44^{lo}CD62L^{hi}$) versus in vitro activated (+4
562 days with anti-CD3/CD28) Tregs. Data from n=5 mice. (B) Fold-change in expression of
563 indicated anti-ferroptotic genes from sorted naive ($CD44^{lo}CD62L^{hi}$) versus in vivo
564 activated ($CD44^{hi}CD62L^{lo}$) Tregs. (C) Fold change in expression of indicated
565 ferroptosis-related genes in 4 day in vitro activated Treg versus Tconv cells. Data from
566 n=5 mice. (D) Treatment of wildtype versus *Aifm2*-deficient Tregs with different
567 concentrations of RSL3 for 4 hours. (E) *Aifm2* expression from bulk RNA-Seq of human
568 PBMCs populations from Database of Immune Cell eQTLs, expression, epigenomics
569 (DICE). (F) Differential expression analysis of *Aifm2* expression across different PBMC
570 populations. For all plots, **P<0.05, **P<0.01, ***P<0.001 by one-way ANOVA (A-B),
571 student t-test (C), or two-way ANOVA (D), mean ± s.e.m (A-C) or mean ± s.d (D).
572
573 **Fig. 3 | Deletion of *Aifm2* in Tregs does not disrupt peripheral tolerance in mice.**
574 (A) Frequency of total $CD8^+$ T cells (left), $CD4^+$ Tconv cells (middle), and Tregs(right) as
575 a percentage of total $CD45^+$ immune cells in lymphoid tissues and organ tissues in 16
576 week mice. (B) Frequencies of activated ($CD44^{hi}CD62^{lo}$) $CD8^+$ T cells (left), $CD4^+$
577 Tconv cells (middle), and Tregs (right) in secondary lymphoid organs (SLOs) in 16
578 week mice. (C) gMFI of Foxp3, CD25, and NRP1 in Foxp3 Tregs across lymphoid
579 tissues and non-lymphoid tissues in 16 week mice. (D) Schematic of pathway for
580 conversion of ATP to Adenosine mediated by CD39 and CD73. (E) Representative
581 histograms and gMFI of CD73 and CD39 in wildtype versus *Aifm2*-deficient Tregs
582 across lymphoid tissues and nonlymphoid tissues in 16 week mice. Data from n=5 for
583 Treg.$Aifm2^{+/+}$ and n=6 for Treg.$Aifm2^{\Delta/\Delta}$ mice for 16 week mice. For all plots, **P<0.05,
584 **P<0.01, ***P<0.001 by two-way ANOVA (A, C, E) or student's t-test (B), mean ±
585 s.e.m.
586
587 **Fig. 4 | Deletion of *Aifm2* in Tregs improves cancer immunity.** (A) Schematic for
588 treating single cell suspensions from MC38 tumors +/- 1μM RSL3 (left). Frequencies of

589 viable $CD8^+$ (left), $CD4^+$ Tconv (middle), and Tregs (right) from tumor single cell
590 suspensions as a percentage of $CD45^+$ cells +/- 1μM RSL3 for 4 hours. Data from n=6
591 mice. (B) Experimental schematic for measuring tumor growth in wildtype versus mice
592 with *Aifm2*-deficient Tregs. (C) Growth of MC38 tumors in wildtype versus mice with
593 *Aifm2*-deficient Tregs. Data from n=5 for Treg.Aifm2$^{+/+}$ and n=6 from *Treg.Aifm2*$^{\Delta/\Delta}$. (D)
594 Frequency of $Foxp3^+$ Tregs as a percentage of total $CD45^+$ immune cells (left) and
595 CD8:Treg ratio (right) in MC38 tumors at D29. (E) Experimental schematic for
596 measuring tumor growth in wildtype versus mice with *Aifm2*-deficient Tregs with or
597 without 10mg/kg liproxstatin injected i.p daily. Data from n=3 for Treg.*Aifm2*$^{+/+}$ + Vehicle,
598 n=4 for Treg.*Aifm2*$^{+/+}$ + Lip-1, n=5 for Treg.*Aifm2*$^{\Delta/\Delta}$+ Vehicle, and n=5 for Treg.*Aifm2*$^{\Delta/\Delta}$
599 + Lip-1. (F) Growth of MC38 tumors in wildtype versus mice with *Aifm2*-deficient Tregs
600 +/- Lip-1. For all plots, **P<0.05, **P<0.01, ***P<0.001 by student t-test (A, D) or two-
601 way ANOVA (C, F), mean ± s.e.m.
602
603 **Fig. 5 | Total T cell deficiency for *Aifm2* preserves $CD8^+$ T cell function and**
604 **improves tumor immunity.** (A) Experimental schematic for measuring tumor growth in
605 wildtype versus mice with *Aifm2*-deficient T cells. (B) Growth of MC38 tumors in
606 wildtype versus mice with *Aifm2*-deficient T cells. Data shown from n=5-6 mice/group
607 from one of two experiments. (C) Frequency of $Foxp3^+$ Tregs as a percentage total
608 $CD45^+$ immune cells in MC38 tumors at D29 from (B). (D) CD8:Treg ratio in MC38
609 tumors at D29 from (B). (E) Representative flow plot for PD-1 and LAG3 staining in total
610 $CD8^+$ T cells (left) and quantification of the frequency of PD-1^+Lag3^+ $CD8^+$ T cells in
611 MC38 tumors (right). (F) Frequency of tumor-specific (MuLV/H2K^{b+}) as a percentage of
612 $CD8^+$ T cells (left) and frequency of PD-1^+Lag3^+ of MuLV/H2K^{b+} $CD8^+$ T cells in MC38
613 tumors (right). For all plots, **P<0.05, **P<0.01, ***P<0.001 by two-way ANOVA (B) or
614 student t-test (C, D, F), mean ± s.e.m.

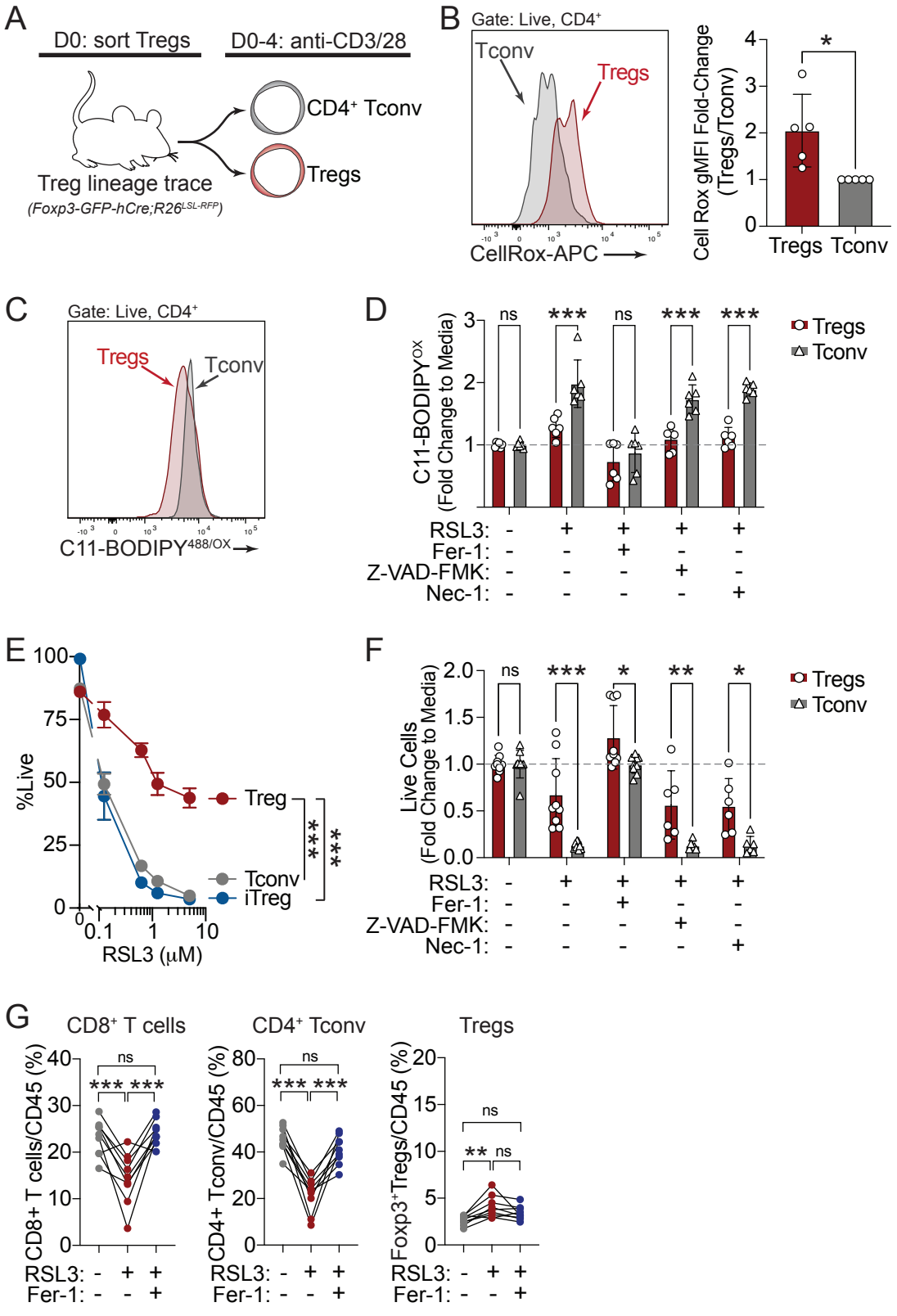

Garcia Castillo J. et al. Fig. 1

Fig. 1 | Regulatory T cells (Tregs) naturally resist lipid peroxide accumulation and ferroptosis. (A) Schematic for *in vitro* T cell assays. (B) Representative flow plots (left) and quantification (right) of bulk reactive oxygen species (ROS) by CellROX™ staining in Tregs versus conventional $CD4^+$ T cells (Tconv) after activation and culture for 4 days *in vitro*. Data pooled from 5 independent experiments. (C) Representative flow plots for detection of oxidized C11-BODIPY in Tregs versus Tconv that were activated for 4 days *in vitro*. (D) Quantification of oxidized C11-BODIPY in Tregs versus Tconv cells *in vitro* +/- 1μM RSL3 in combination with 2μM Fer-1, 100μM Z-VAD-FMK, or 10μM Nec-1. Data pooled from 3 experiments. (E) Cell viability of Tregs (nTregs), $CD4^+$ Tconv, and induced Tregs ($Foxp3^+$ iTregs) treated with the indicated concentrations of RSL3 for 4 hours. Representative data from 2 independent experiments. (F) Cell viability of Tregs versus $CD4^+$ Tconv treated *in vitro* +/- 1μM RSL3 in combination with 2μM Fer-1, 100μM Z-VAD-FMK, or 10μM Nec-1. Data pooled from 2 experiments. (G) Frequencies of viable $CD8^+$ T (left), $CD4^+$ Tconv (middle), and Tregs (right) from spleen plotted as the percent of $CD45^+$ cells +/- 1μM RSL3 and 2μM Fer-1. Data from n=7 mice. For all plots, **P<0.05, **P<0.01, ***P<0.001 by two-way ANOVA (D-F) or one-way ANOVA (G), or student t-test (B), mean ± s.d (B, D-F) or mean ± s.e.m (G).

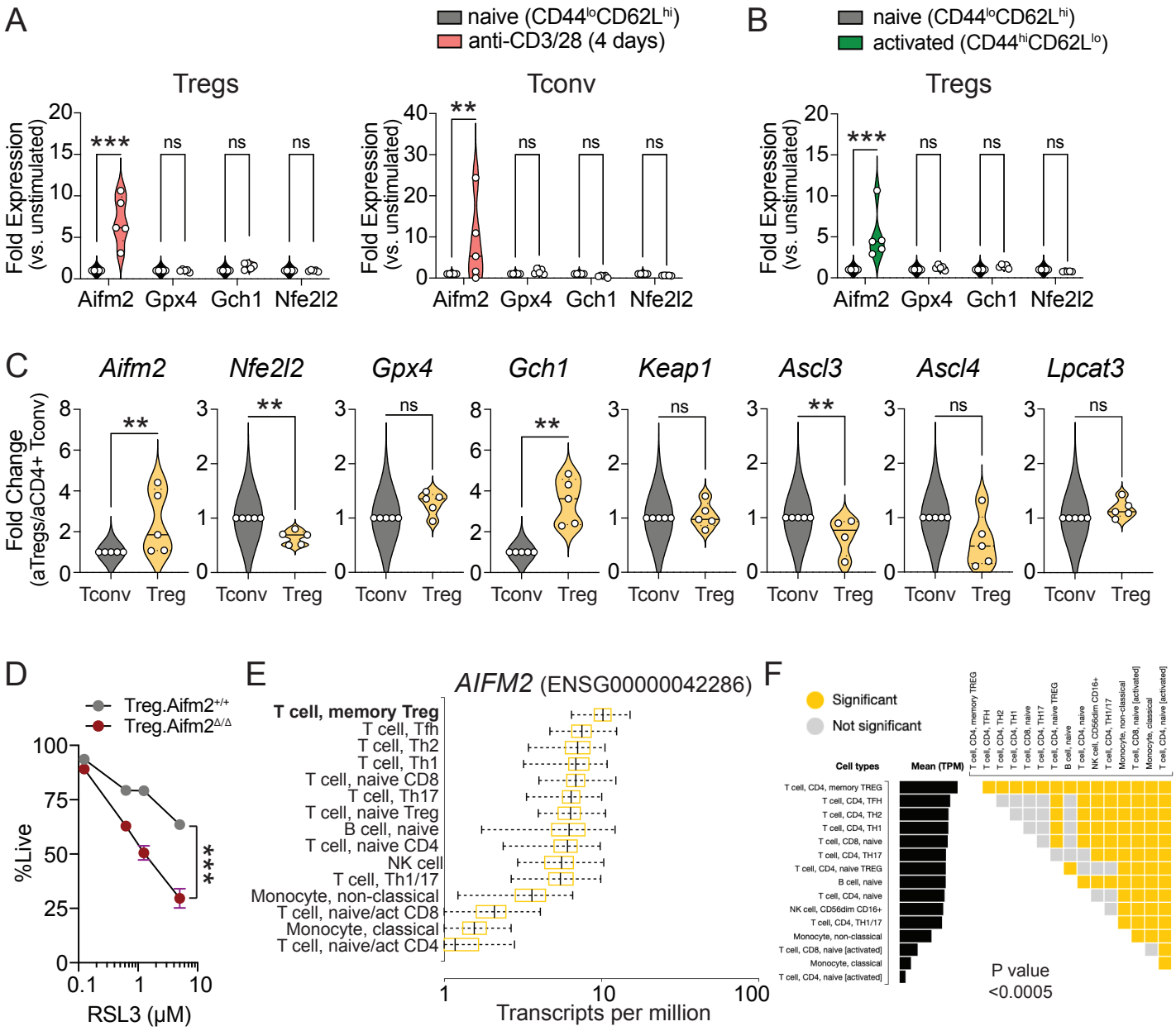

Garcia Castillo, J. et al. Fig. 2.

Fig. 2 | FSP1 drives Treg resistance to ferroptosis. (A) Fold-change expression of indicated anti-ferroptotic genes in naive ($CD44^{lo}CD62L^{hi}$) versus in vitro activated (+4 days with anti-CD3/CD28) Tregs. Data from n=5 mice. (B) Fold-change in expression of indicated anti-ferroptotic genes from sorted naive ($CD44^{lo}CD62L^{hi}$) versus in vivo activated ($CD44^{hi}CD62L^{lo}$) Tregs. (C) Fold change in expression of indicated ferroptosis-related genes in 4 day in vitro activated Treg versus Tconv cells. Data from n=5 mice. (D) Treatment of wildtype versus *Aifm2*-deficient Tregs with different concentrations of RSL3 for 4 hours. (E) *Aifm2* expression from bulk RNA-Seq of human PBMCs populations from Database of Immune Cell eQTLs, expression, epigenomics (DICE). (F) Differential expression analysis of *Aifm2* expression across different PBMC populations. For all plots, **P<0.05, **P<0.01, ***P<0.001 by one-way ANOVA (A-B), student t-test (C), or two-way ANOVA (D), mean ± s.e.m (A-C) or mean ± s.d (D).

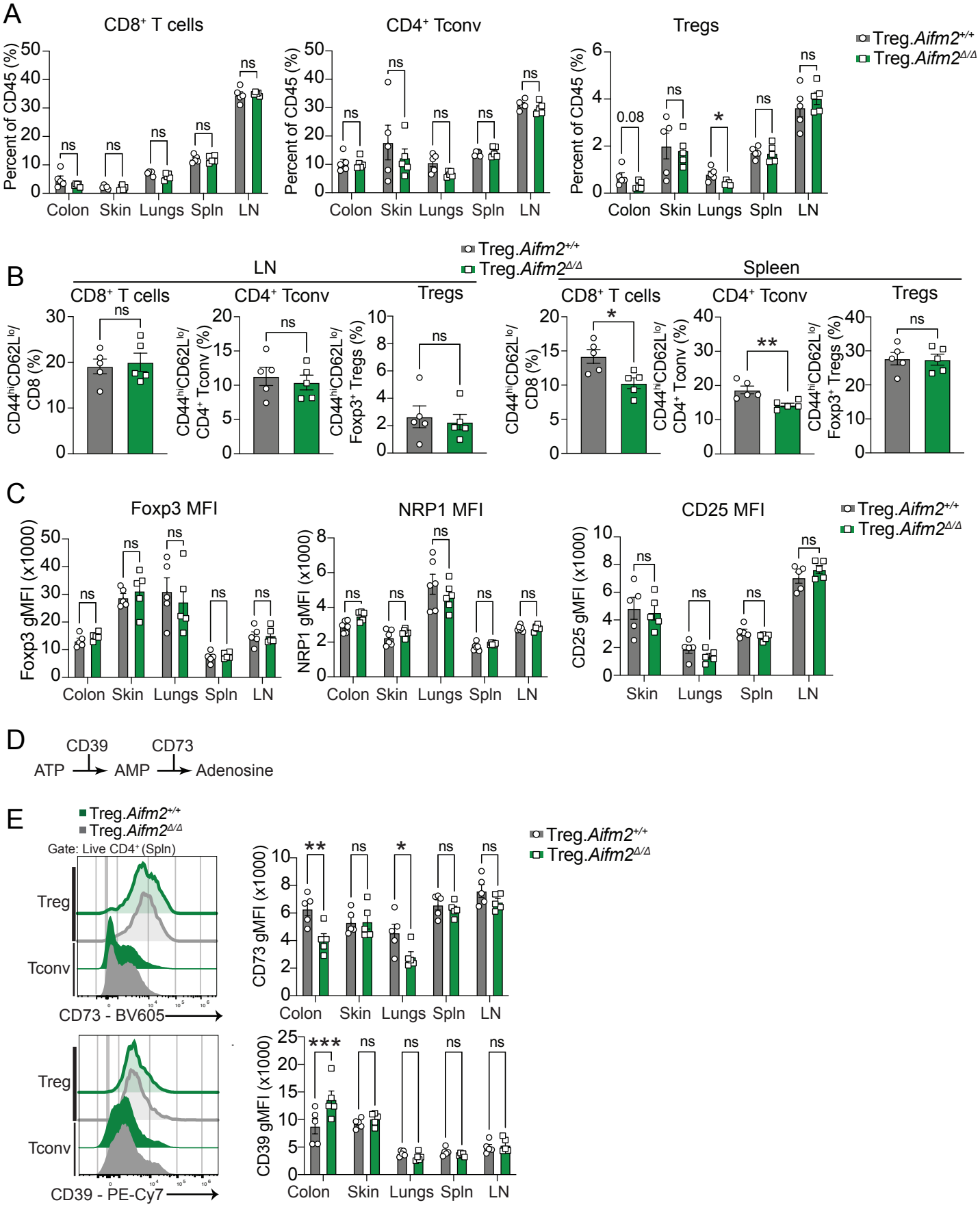

Garcia Castillo, J. et al. Fig. 3.

Fig. 3 | Deletion of *Aifm2* in Tregs does not disrupt peripheral tolerance in mice. (A) Frequency of total $CD8^+$ T cells (left), $CD4^+$ Tconv cells (middle), and Tregs(right) as a percentage of total $CD45^+$ immune cells in lymphoid tissues and organ tissues in 16 week mice. (B) Frequencies of activated ($CD44^{hi}CD62^{lo}$) $CD8^+$ T cells (left), $CD4^+$ Tconv cells (middle), and Tregs (right) in secondary lymphoid organs (SLOs) in 16 week mice. (C) gMFI of Foxp3, CD25, and NRP1 in Foxp3 Tregs across lymphoid tissues and non-lymphoid tissues in 16 week mice. (D) Schematic of pathway for conversion of ATP to Adenosine mediated by CD39 and CD73. (E) Representative histograms and gMFI of CD73 and CD39 in wildtype versus *Aifm2*-deficient Tregs across lymphoid tissues and nonlymphoid tissues in 16 week mice. Data from n=5 for Treg.*Aifm2*$^{+/+}$ and n=6 for Treg.*Aifm2*$^{\Delta/\Delta}$ mice for 16 week mice. For all plots, **P<0.05, **P<0.01, ***P<0.001 by two-way ANOVA (A, C, E) or student's t-test (B), mean ± s.e.m.

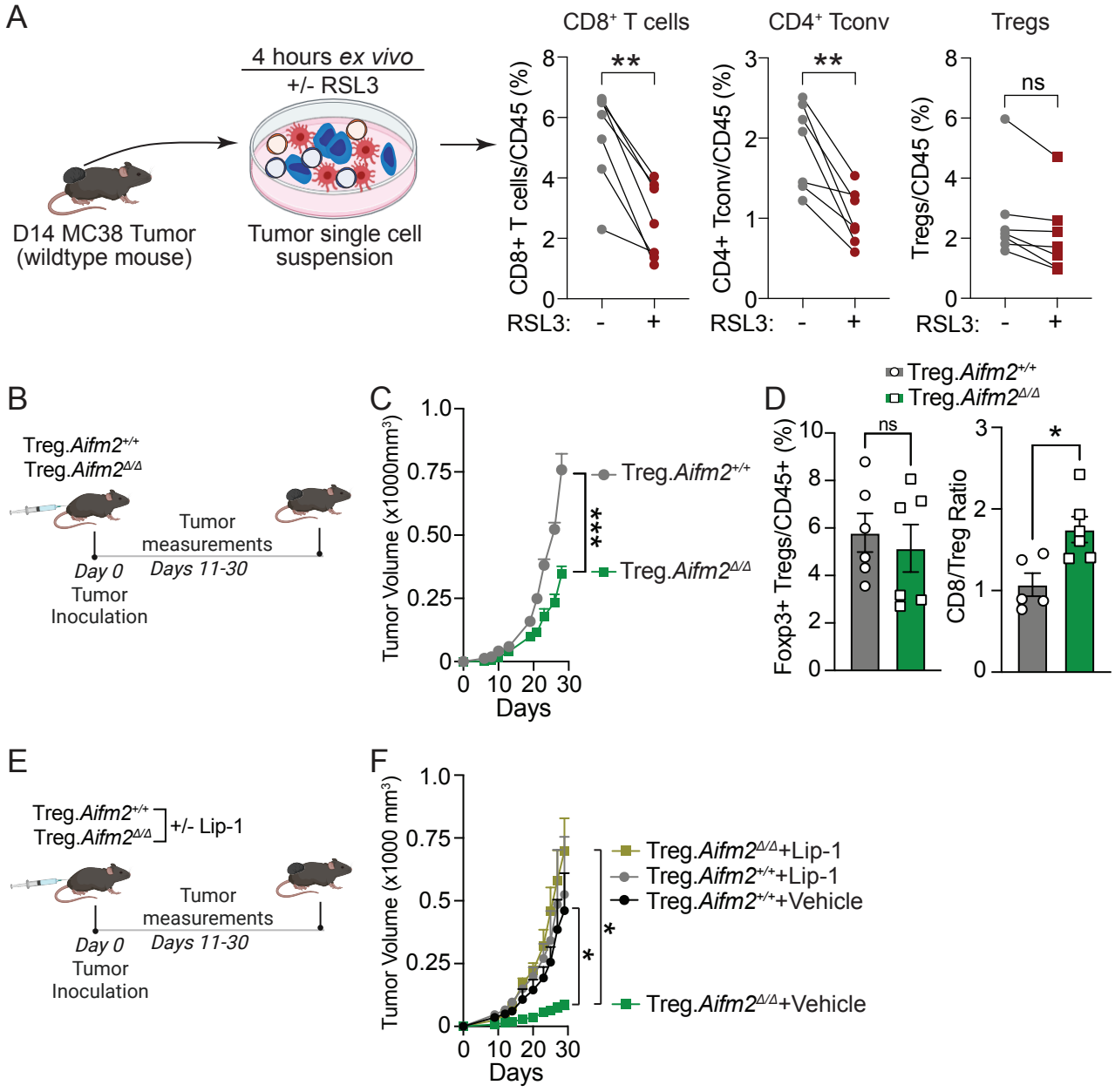

Garcia Castillo, J. et al. Fig. 4.

Fig. 4 | Deletion of *Aifm2* in Tregs improves cancer immunity. (A) Schematic for treating single cell suspensions from MC38 tumors +/- 1μM RSL3 (left). Frequencies of viable $CD8^+$ (left), $CD4^+$ Tconv (middle), and Tregs (right) from tumor single cell suspensions as a percentage of $CD45^+$ cells +/- 1μM RSL3 for 4 hours. Data from n=6 mice. (B) Experimental schematic for measuring tumor growth in wildtype versus mice with *Aifm2*-deficient Tregs. (C) Growth of MC38 tumors in wildtype versus mice with *Aifm2*-deficient Tregs. Data from n=5 for Treg.Aifm2$^{+/+}$ and n=6 from *Treg.Aifm2*$^{\Delta/\Delta}$. (D) Frequency of $Foxp3^+$ Tregs as a percentage of total $CD45^+$ immune cells (left) and CD8:Treg ratio (right) in MC38 tumors at D29. (E) Experimental schematic for measuring tumor growth in wildtype versus mice with *Aifm2*-deficient Tregs with or without 10mg/kg liproxstatin injected i.p daily. Data from n=3 for Treg.*Aifm2*$^{+/+}$ + Vehicle, n=4 for Treg.*Aifm2*$^{+/+}$ + Lip-1, n=5 for Treg.*Aifm2*$^{\Delta/\Delta}$+ Vehicle, and n=5 for Treg.*Aifm2*$^{\Delta/\Delta}$ + Lip-1. (F) Growth of MC38 tumors in wildtype versus mice with *Aifm2*-deficient Tregs +/- Lip-1. For all plots, **P<0.05, **P<0.01, ***P<0.001 by student t-test (A, D) or two-way ANOVA (C, F), mean ± s.e.m.

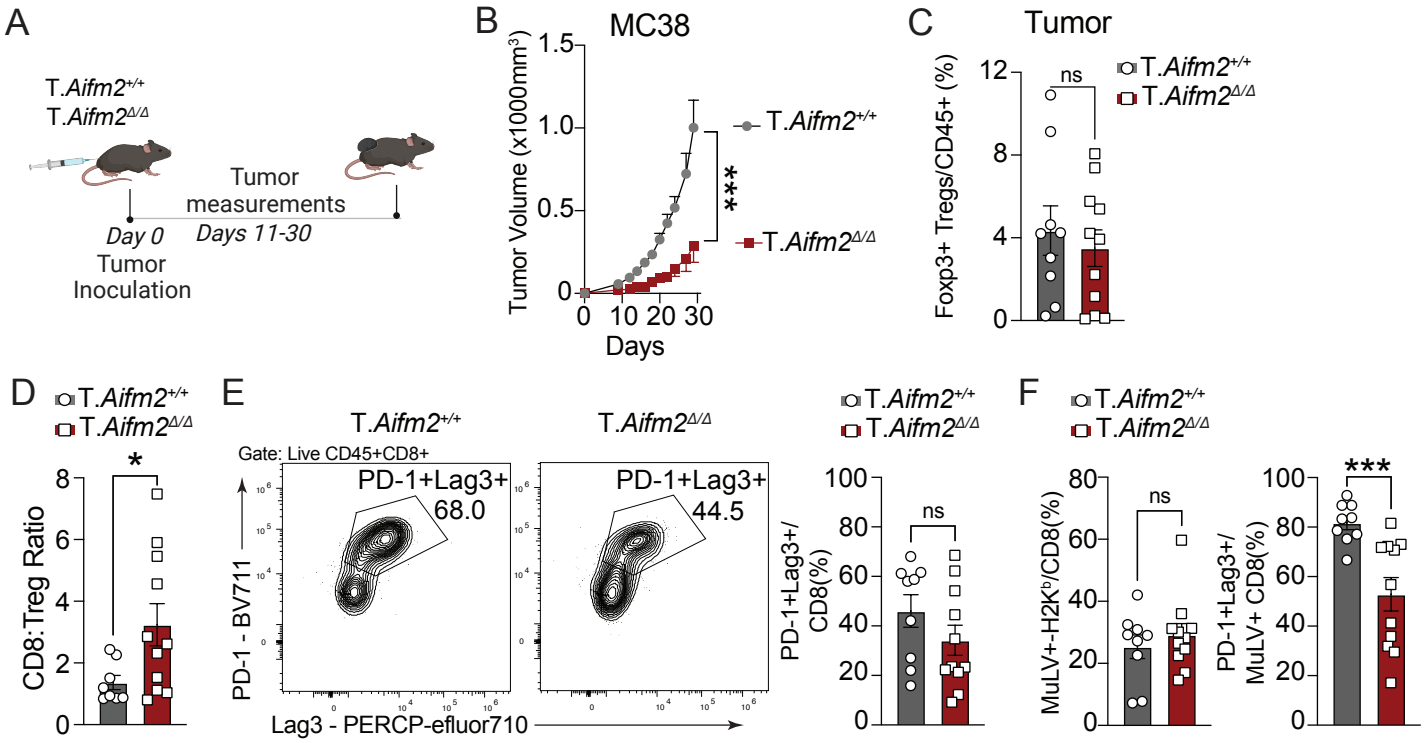

Garcia Castillo, J. Fig. 5

Fig. 5 | Total T cell deficiency for *Aifm2* preserves CD8$^+$ T cell function and improves tumor immunity. (A) Experimental schematic for measuring tumor growth in wildtype versus mice with *Aifm2*-deficient T cells. (B) Growth of MC38 tumors in wildtype versus mice with *Aifm2*-deficient T cells. Data shown from n=5-6 mice/group from one of two experiments. (C) Frequency of Foxp3$^+$ Tregs as a percentage total CD45$^+$ immune cells in MC38 tumors at D29 from (B). (D) CD8:Treg ratio in MC38 tumors at D29 from (B). (E) Representative flow plot for PD-1 and LAG3 staining in total CD8$^+$ T cells (left) and quantification of the frequency of PD-1$^+$Lag3$^+$ CD8$^+$ T cells in MC38 tumors (right). (F) Frequency of tumor-specific (MuLV/H2K^{b+}) as a percentage of CD8$^+$ T cells (left) and frequency of PD-1$^+$Lag3$^+$ of MuLV/H2K^{b+} CD8$^+$ T cells in MC38 tumors (right). For all plots, **P<0.05, **P<0.01, ***P<0.001 by two-way ANOVA (B) or student t-test (C, D, F), mean ± s.e.m.